

AbFlow : End-to-end Paratope-Centric Antibody Design by Interaction Enhanced Flow Matching

Wenda Wang

wangwenda87@ruc.edu.cn

Renmin University of China, Beijing, China

Zhewei Wei

zhewei@ruc.edu.cn

Renmin University of China, Beijing, China

Yang Zhang

fengyuewuya@ruc.edu.cn

China National Institute of Standardization, Beijing, China

Renmin University of China, Beijing, China

Wenbing Huang

hwenbing@126.com

Renmin University of China, Beijing, China

Abstract

Antigen-antibody binding is a critical process in the immune response. Although recent progress has advanced antibody design, current methods lack a generative framework for end-to-end modeling of full-atom antibody structures and struggle to fully exploit antigen-specific geometric information for optimizing local binding interfaces and global structures. To overcome these limitations, we introduce AbFlow, a flow-matching framework that leverages optimal transport to design full-atom antibodies end-to-end. AbFlow incorporates an extended velocity field network featuring an equivariant Surface Multi-channel Encoder, which uses surface-level antigen interaction data to refine the antibody structure, particularly the CDR-H3 region. Extensive experiments in paratope-centric antibody design, multi-CDRs and full-atom antibody design, binding affinity optimization, and complex structure prediction show that AbFlow produces superior antigen-antibody complexes, especially at the contact interface, and markedly improves the binding affinity of generated antibodies.

CCS Concepts

- Applied computing → Molecular structural biology; Bioinformatics;
- Computing methodologies → Neural networks.

Keywords

Antibody Design; Flow Matching; Equivariant Graph Neural Network; Surface Modeling

ACM Reference Format:

Wenda Wang, Yang Zhang, Zhewei Wei, and Wenbing Huang. 2026. AbFlow : End-to-end Paratope-Centric Antibody Design by Interaction Enhanced Flow Matching. In *Proceedings of the 32nd ACM SIGKDD Conference on Knowledge Discovery and Data Mining V.1 (KDD '26)*, August 09–13, 2026,

Zhewei Wei is the corresponding author. The work was partially done at Gaoling School of Artificial Intelligence, Beijing Key Laboratory of Research on Large Models and Intelligent Governance, Engineering Research Center of Next-Generation Intelligent Search and Recommendation, MOE, and Pazhou Laboratory (Huangpu), Guangzhou, Guangdong 510555, China.

KDD '26, Jeju Island, Republic of Korea

© 2026 Copyright held by the owner/author(s).

This is the author's version of the work. It is posted here for your personal use. Not for redistribution. The definitive Version of Record was published in *Proceedings of the 32nd ACM SIGKDD Conference on Knowledge Discovery and Data Mining V.1 (KDD '26)*, August 09–13, 2026, Jeju Island, Republic of Korea, <https://doi.org/10.1145/3770854.3780296>.

Jeju Island, Republic of Korea. ACM, New York, NY, USA, 12 pages. <https://doi.org/10.1145/3770854.3780296>

Resource Availability:

The source code of this paper has been made publicly available at <https://doi.org/10.5281/zenodo.18085636>.

Our code is also available at <https://github.com/WangWenda87/AbFlow.git> for direct access and updates.

1 Introduction

Antibodies can specifically recognize and bind to antigens, thus playing multiple immune defense functions, such as neutralizing the toxicity of pathogens and marking pathogens for clearance by immune cells [7]. The design of antibodies for specific antigens is significant in biology and immunology [5, 9, 43]. However, due to the key binding role and high variability of the complementarity-determining regions (CDRs) of antibodies, this task is often challenging [12, 46, 47].

Antibody design involves the joint generation of an antibody's complete sequence and full-atom structure. Traditional energy-based optimization [8, 24] was initially applied. Later, 1D sequence learning-based language models [26, 37] emerged, characterized by their ability to model antibody sequences linearly, focusing on capturing patterns and relationships within amino acid sequences without considering the 3D structural context.

Recent antibody design approaches can be broadly classified into step-by-step pipelines and end-to-end generative methods. Step-by-step methods decompose the antibody design task into sequential stages, with models tailored to specific sub-problems—typically focusing on CDR design, particularly CDR-H3. These methods generally follow a fixed pipeline: starting from predicting the antibody structure from its sequence [36], docking the antibody and antigen structures [34, 49], then generating or predicting CDR-H3 sequences and structures [18, 21, 28, 53], and finally performing side-chain packing based on residue identity and geometry [4]. Among these, MEAN [21] and HERN [18] adopt GNN-based predictive frameworks, while DiffAb [28] and AbX [53] utilize diffusion-based generative modeling for CDR synthesis.

In contrast, end-to-end methods [22, 45] aim to model the antibody design process holistically. Given a specific antigen and a partial antibody sequence lacking the CDR-H3, these methods directly generate the complete antibody sequence and full-atom 3D structure in a single, unified framework. For example, dyMEAN

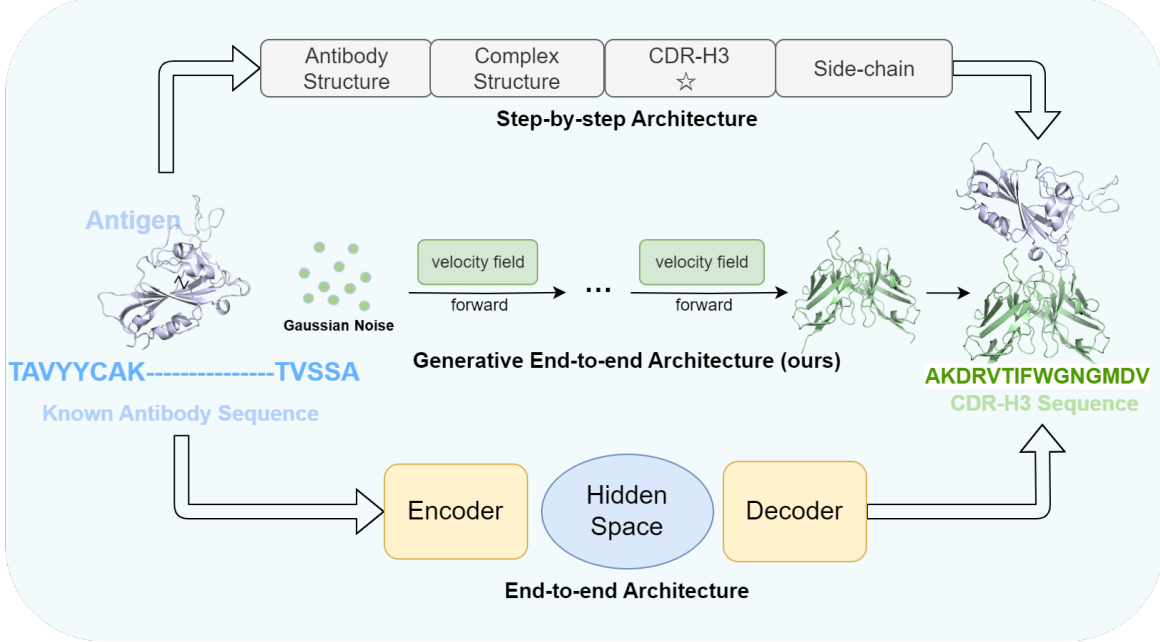


Figure 1: Overall illustration of antibody design algorithm. Given antibody sequences lacking CDR-H3, generate complete sequences and 3D structures. Unlike existing methods that mostly focus on a single step (e.g., CDR-H3 generation) in antibody design tasks and a few end-to-end frameworks, we propose a novel generative end-to-end architecture.

[22] performs full-atom generation through modules including antibody initialization, multi-channel equivariant encoding, and joint sequence-structure prediction. Recent methods further realize end-to-end design via flow matching: dyAb [44] generates CDR sequences and structures during a fine-grained optimization stage before grafting them onto a coarse-grained template, while IgFlow [32] performs joint discrete-continuous flow matching on the entire antibody to produce coupled sequence-structure designs.

Despite significant progress in antibody design, two critical challenges persist. **First, current generative frameworks insufficiently integrate sequence-structure generation with global geometric message passing.** Existing models either perform local (e.g., CDR or paratope) antibody structure generation, but generally fail to model the structural information flow between the paratope and the rest of the antibody or to account for holistic structural refinement, resulting in weak coupling between generative dynamics and structural information propagation [28, 53]. **This decoupling limits their ability to produce globally coherent full-atom antibodies.**

Second, the inability to leverage fine-grained antigen geometry for precise interface modeling. Current models struggle to utilize detailed geometric features of the antigen surface, limiting their ability to accurately model antigen-antibody interfaces [52]. This shortcoming impairs structural signal propagation across the antibody framework, leading to suboptimal interface complementarity and reduced global structural coherence in generated antibodies.

Based on the aforementioned research progress and challenges, we propose **AbFlow**, a novel flow-based generative framework for end-to-end full-atom antibody design. Our main contributions are as follows:

- Our AbFlow employs a **paratope-restricted flow matching module** for efficient high-fidelity generation. The framework incorporates an **EGNN-based joint generative and message-passing velocity field** that both drives paratope flow dynamics and propagates structural information from the generated paratope to the full antibody. This dual functionality enables coherent full-atom refinement of the entire antibody despite applying flow only to a local region.
- To address the lack of antigen-specific geometric context in existing methods, we propose an **equivariant Surface Multi-channel Encoder (SME)** that extracts fine-grained structural cues from the antigen surface. This geometric information is subsequently injected into the velocity field network to effectively guide paratope generation in an antigen-aware and interaction-consistent manner.
- Extensive experiments on **paratope-centric antibody design, multi-CDRs and full-atom antibody design, binding affinity optimization, and complex structure prediction** demonstrate that our AbFlow outperforms existing step-by-step and end-to-end baselines in structural accuracy, interface quality, and binding affinity.

See Figure 1 for a schematic comparison of different antibody design paradigms, including step-by-step pipelines, conventional end-to-end frameworks, and our generative approach.

2 Related Work

Antibody design. Antibody aims to develop antibodies that can bind to specific antigens with high efficiency. Based on the diffusion probabilistic model, DiffAb [28] iteratively updates the amino acid type, position, and orientation of CDRs to achieve tasks such as sequence-structure co-design. HERN [18] employs a hierarchical equivariant refinement network. The paratope docking task predicts atomic forces through a hierarchical message passing network. MEAN [21] models antibody design as a 3D-equivariant graph translation problem, with the multi-channel equivariant attention network and the progressive full-shot decoding strategy. dyMEAN [22], an end-to-end full-atom model, through an adaptive multi-channel encoder, iteratively updates the antibody sequence and structure. Our work further develops this end-to-end method, enhancing the quality of the interaction between the generated antibody and the antigen, as well as their binding affinity.

Generative model. In recent years, generative models, including diffusion-based and flow-based models, have been increasingly used in molecular and protein generation tasks. AlphaFold 3 [1] replaces the structure module of AlphaFold 2 [19] with a diffusion module for generating 3D structures. DiffAb [28] and AbX [53] are based on DDPM [15] and score-based models [40], respectively, for antibody CDR design. Flow matching [3, 25, 27] simulates the transport from a simple distribution to the target (data) distribution by learning Continuous Normalizing Flows (CNFs). Flow matching has recently gained widespread use in molecular generation tasks. ETFlow [14] implements molecular 3D conformer optimization based on flow matching, while GOAT [16] combines flow and optimal transport theory for 3D molecular generation. In our work, we apply the local flow matching framework to end-to-end antibody design tasks.

Surface representation. The structure surface contains the geometric and chemical information that reflects the interaction patterns and relationship with other molecules. MaSIF [13, 42] decomposes the surface into overlapping radial patches, extracts features, and embeds them into vector descriptors, applying them to various tasks with the help of geometric deep learning. EquiPocket [51] treats proteins as graph structures, extracting atomic geometric information and predicting ligand binding sites using an E(3)-equivariant graph neural network for modeling and message passing. SurfPro [41] models surface features with a hierarchical encoder and generates amino acid sequences with an autoregressive decoder. We introduce surface representation into the antibody design task to convey more fine-grained interaction information between the antigen and the antibody.

3 Notations and Problem Setting

A general antibody has a characteristic Y-shaped structure composed of two heavy chains and two light chains held together by disulfide bonds. It has constant domains that remain unchanged among different antibodies, and variable regions at the tips of the Y that specifically recognize and bind to antigens.

Our work lies in the variable regions $V = \{V_h, V_l\}$, where V_h and V_l represent the variable regions in the heavy and light chains. A variable region can be divided into four framework regions (FRs) and three complementarity-determining regions (CDRs). In work

related to antibody design, CDR design refers to the design of the coordinates and sequence of the third complementarity-determining region (CDR-H3) of the heavy chain. Since the sequence of this part of the antibody is highly variable and often unknown, it dominates the binding of antigen and antibody [29]. In this paper, we refer to CDR-H3 as the **paratope** according to [18]. Additionally, the part of an antigen that binds to the antibody is called the **epitope**.

Following [21] and [22], we use the graph format $\mathcal{G} = (\mathcal{V}, \mathcal{E})$ to represent the epitope and paratope used in this work. Here, node set \mathcal{V} consists of all residues in the structure, where $\mathcal{V} = \{v_i\}_{i=1}^{|\mathcal{V}|}$ and $v_i = (a_i, X_i)$. In this, $a_i \in \mathbb{R}$ represents the type of the i -th amino acid, and $X_i \in \mathbb{R}^{3 \times c_i}$ represents the full-atom 3D coordinates of the residue, where c_i indicates the number of atoms in this residue. As a full-atom design method, we need to represent the different numbers of atoms in different residues. The edge set \mathcal{E} is calculated based on the distances between nodes in \mathcal{G} . We calculate the pairwise distance between two residues v_i and v_j as Equation (1) :

$$d(v_i, v_j) = \min_{1 \leq m \leq c_i, 1 \leq n \leq c_j} \|X_i(:, m) - X_j(:, n)\|_2. \quad (1)$$

Here, $X_i(:, m)$ and $X_j(:, n)$, respectively, represent the m -th atom of residue i and the n -th atom of residue j . Then, we calculate the k -nearest neighborhood (KNN) of each residue. In this way, we can define epitope $\mathcal{G}_E = (\mathcal{V}_E, \mathcal{E}_E)$, antibody $\mathcal{G}_A = (\mathcal{V}_A, \mathcal{E}_A)$ and paratope $\mathcal{G}_P = (\mathcal{V}_P, \mathcal{E}_P)$.

Problem Setting: The main task of our work is to design the full-atom antibody 3D structures as well as the paratope sequences under the premise that only the epitope is known and the sequence of the antibody without the CDR-H3 part is available. Expressed in symbols: Given the epitope $\mathcal{G}_E = (\mathcal{V}_E, \mathcal{E}_E)$ and the antibody sequence with missed paratope $\{a_i | i \in \mathcal{V}_A, i \notin \mathcal{V}_P\}$, design paratope sequences $\{a_i | i \in \mathcal{V}_P\}$ and full-atom antibody 3D coordinates $\{X_i | i \in \mathcal{V}_A\}$.

Beyond this basic problem setting, AbFlow can be naturally extended to a broader range of antibody modeling tasks. In particular, we demonstrate the scalability of our framework through applications to multi-CDRs design and antigen-antibody complex structure prediction, highlighting its flexibility and generality across different antibody modeling scenarios.

4 Method

Figure 2 presents an overview of our AbFlow method. Next, we will provide a detailed introduction to each module in the architecture. Section 4.1 discusses the definition of the flow matching framework applied in antibody structures and the process of paratope distribution’s transport. Section 4.2 introduces the definition and sampling of the epitope surface. And section 4.3 presents the extended velocity field network, including Surface Multi-Channel Encoder (SME) used to enhance the interaction between epitope and paratope information, as well as the network that propagates structural information from the paratope to the entire antibody. Section 4.4 presents the training loss and algorithms of training and sampling.

4.1 Flow Matching with Optimal Transport

To address the absence of flow-based frameworks in existing antibody design models, we propose to model antibody structure

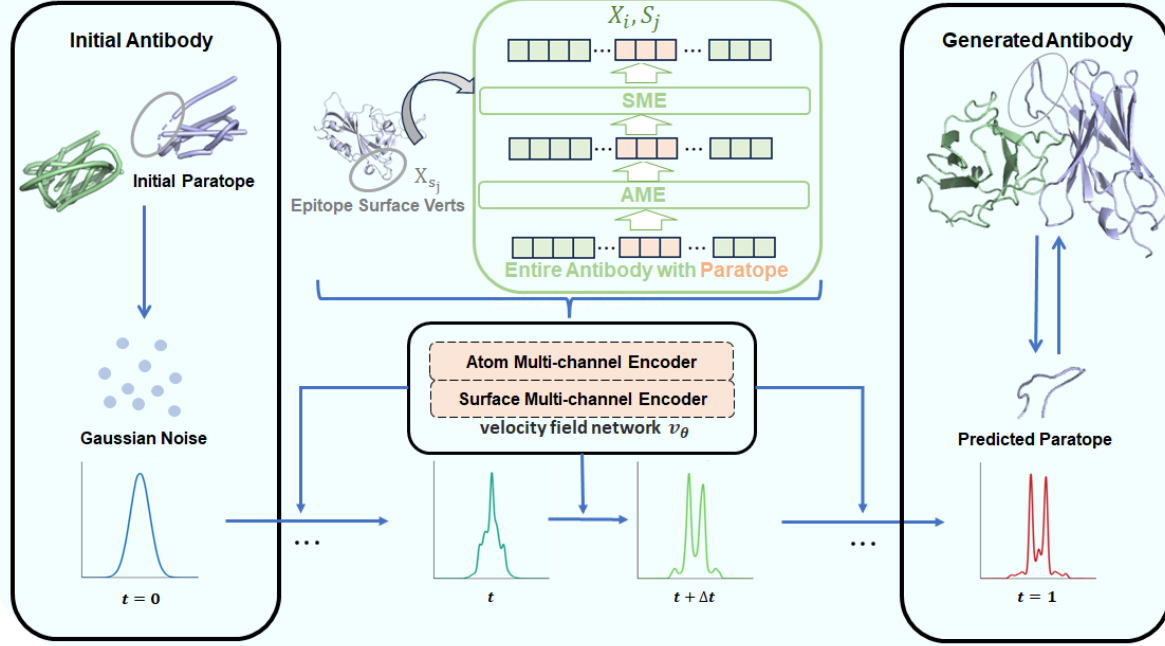


Figure 2: Overall architecture of AbFlow. Input the antigen epitope and the antibody sequence lacking CDR-H3 as introduced in Section 3. We extract the paratope as the flow for the transport of probability distribution. In the single-step forward process, we introduce an extended velocity field network that not only predicts flow dynamics but also enhances specific-antigen binding interface information through a Surface Multi-channel Encoder (SME), propagating this information from the paratope to the entire antibody structure.

distributions through continuous normalizing flows (CNFs). But the direct application of CNFs to a complete antibody will result in a calculation efficiency problem due to the large 3D structure. To resolve this bottleneck, we strategically constrain the CNFs to focus solely on paratope structures $X = \{X_i | i \in \mathcal{V}_p\}$. The aim is to learn a time-dependent velocity field $u(x, t) : \mathbb{R}^{N \times 3} \times [0, 1] \rightarrow \mathbb{R}^{N \times 3}$ associated with the transport map $X_t : \mathbb{R}^{N \times 3} \times [0, 1] \rightarrow \mathbb{R}^{N \times 3}$ that can guide samples transport from a simple distribution, we use Gaussian noise in our work, to a target data distribution that represents true paratope structures. Sampling can be achieved by solving ordinary differential equations (ODEs) as shown in Equation (2).

$$X_{t+\Delta t} = u(X_t, t), X_0 = x_0 \sim \rho_0. \quad (2)$$

Here, x_0 refers to the initial samples from the Gaussian distribution. We can construct the conditional probability path $p(x_t | x_1)$ and predict the conditional velocity field $u(x_t | x_1)$. We consider the Gaussian conditional probability path:

$$\rho_t(x | x_1) = \mathcal{N}(x_t | \mu_t(x_1), \sigma_t^2(x_1)I). \quad (3)$$

Then the flow $\psi_t(x)$ can be considered as the affine transformation that maps to $\rho_t(x | x_1)$ conditioned on x_1 :

$$\psi_t(x) = \sigma_t(x_1)x + \mu_t(x_1). \quad (4)$$

According to the Wasserstein-2 optimal transport solution [11, 33], we formulate the conditional probability path $\rho_t(x | x_1)$ using the mean and standard deviation that vary linearly over time, as shown in the Equation (5):

$$\mu_t(x_1) = tx_1, \sigma_t(x_1) = 1 - (1 - \sigma_{\min})t. \quad (5)$$

Consequently, the flow can be expressed as $\psi_t(x) = [1 - (1 - \sigma_{\min})t]x + tx_1$. The state of the flow at time t , $x_t = \psi_t(x_0)$, can also be interpreted as a linear interpolation between x_0 and x_1 . The loss function of the CFM can be regarded as a regression prediction of the true velocity field, which is obtained by differentiating the flow with respect to t , as shown in Equation (6):

$$\mathcal{L}_{\text{CFM}}(\theta) = \mathbb{E}_{t \sim U[0,1], x_0, x_1 \sim \Gamma(\rho_0, \rho_1)} \|v_\theta(x_t) - (x_1 - (1 - \sigma_{\min})x_0)\|^2. \quad (6)$$

Where U is a Uniform distribution, $\Gamma(\cdot, \cdot)$ is a coupling distribution, and ρ_0 and ρ_1 are respectively the marginal distributions of Γ with respect to x_1 and x_0 . v_θ represents the network that fits the true velocity field.

It is also worth noting that, inspired by Rectified Flow [27], to avoid trajectory crossings that may occur from interpolating randomly paired samples drawn from two distributions, we adopt a method of **pre-aligning the sample pairs**. Specifically, we solve

for the transition, rotation, and permutation that minimize the structural distance between the Gaussian noise and paratope samples, i.e., $\arg \min_{R, t, \pi} \|x_1 - \pi(Rx_0 + t)\|^2$. We use the Kabsch algorithm [20] to compute the optimal translation \vec{t} and optimal rotation \vec{R} , and the Hungarian algorithm [23] to compute the optimal permutation $\vec{\pi}$. Accordingly, the noise samples paired with corresponding paratope samples are given by $\hat{x}_0 = \vec{\pi}(\vec{R}x_0 + \vec{t})$. The flow loss we ultimately use can be formulated as Equation (7):

$$\mathcal{L}_F = \mathbb{E}_{t \sim U[0,1], x_0, x_1 \sim \Gamma(\rho_0, \rho_1)} \|v_\theta(x_t) - (x_1 - (1 - \sigma_{\min})\hat{x}_0)\|^2. \quad (7)$$

The above describes our flow matching framework based on optimal transport. In the following, we will introduce the design of the predicted velocity field network architecture.

4.2 Surface Definition and Sampling

In this section, we describe the procedure for constructing surface vertices around the epitope and sampling representative points for interaction with the paratope. Since the paratope inherently forms a flexible and well-defined surface on the antibody, we focus exclusively on modeling the surface of the epitope to enhance the message passing between the antigen and antibody.

Given the epitope residues $\{X_i \mid i = 1, 2, \dots, N = |\mathcal{V}_E|\}$, we utilize MSMS [38] to generate a dense set of surface vertices $\mathbb{S} = \{s_1, s_2, \dots, s_M\}$ within a radius of 1.5 \AA centered on the epitope region, where $M \gg N$. For each vertex $s_i \in \mathbb{S}$, we assign an *attribution residue* by identifying its nearest epitope residue according to the following rule:

$$v_j = \arg \min_{1 \leq k \leq N} \|s_i - X_k\|_2.$$

This association partitions the vertex set \mathbb{S} into N disjoint subsets, each corresponding to an epitope residue:

$$\mathbb{S}_{v_p} = \{s_q\}_{q=1}^{m_p}, \quad p = 1, \dots, N, \quad (8)$$

$$\sum_{p=1}^N m_p = M, \quad 0 \leq m_p \ll M. \quad (9)$$

To reduce computational cost and maintain robustness across residues, we randomly sample at most M_0 surface vertices for each epitope residue before each round of message passing. These sampled vertices are then used to interact with the paratope, injecting local geometric and chemical information from the antigen surface into the antibody representation. Notably, we avoid using all available vertices or a multi-channel aggregation strategy, as the number of vertices associated with each epitope residue varies significantly and can become prohibitively large in practice.

4.3 SME and Velocity Field Network

Next, to address the challenge that specific antigen structure information is underutilized in guiding antibody design, we propose a Surface Multi-channel Encoder (SME) to propagate finer-grained, surface-level epitope information to paratope structures. SME can uniformly handle residues with different channel sizes on the paratope as well as surface vertices on the epitope surface, whose size is far larger than the channel size of residues. It can also effectively capture the geometric context between surface vertices and residue atoms, enabling fine-grained message construction.

By aggregating these geometry-aware messages, the SME module **facilitates directional information from the epitope surface to the antibody paratope**. The process of a single update can be represented by Equation (10)–(14).

$$m_{ij} = \phi_m \left(S_i^{(l)}, S_j^{(l)}, \text{msg}(X_i^{(l)}, X_{s_j}^{(l)}) \right), \quad (10)$$

$$\text{msg}(X_i^{(l)}, X_{s_j}^{(l)}) = \frac{\phi_v \left(A_i^T D(X_i^{(l)}, X_{s_j}^{(l)}) \right)}{\|D(X_i^{(l)}, X_{s_j}^{(l)})\|_F + \epsilon}, \quad (11)$$

$$X_{ij} = \sum_{k=1}^M \left(X_i^{(l)} - \mathbf{1} X_{s_j}^{(l)} [k, :] \right), \quad (12)$$

$$S_i^{(l+1)} = \phi_s \left(S_i^{(l)}, \sum_{j \in \mathcal{N}_i} m_{ij} \right), \quad (13)$$

$$X_i^{(l+1)} = X_i^{(l)} + \frac{1}{|\mathcal{N}_i|} \sum_{j \in \mathcal{N}_i} X_{ij} \phi_x(m_{ij}). \quad (14)$$

Where S_i, X_i are the sequence and coordinate representation of the i -th residue node, respectively, $X_{s_j} \in \mathbb{R}^{M \times 3}$ represents the coordinates of surface vertices belonging to the j -th residue. \mathcal{N}_i represents the neighbor of residue i , ϕ_m, ϕ_v, ϕ_x are different MLP layers, and $\mathbf{1}$ is a vector of all ones. $D(\cdot, \cdot)$ is the calculation of the pair-wise Euclidean distance of two matrices. For the learnable attribute matrix $A_i \in \mathbb{R}^{c_i \times d}$, the vector of each row is learned from the type and position of the corresponding i -th atom. We discuss and prove the E(3)-equivariance of SME in Appendix A.

The SME module is integrated into the velocity field network v_θ , enabling it to jointly predict flow dynamics and propagate antigen-specific messages across the antibody structure. To construct v_θ , we combine SME with the Atom Multi-channel Encoder (AME) from [22], forming a hybrid message-passing backbone. While SME focuses on fine-grained surface-level transmission of antigen-epitope information to the paratope (critical for binding affinity), AME handles global structural propagation. This design allows localized paratope flow modeling while retaining full-atom generation capabilities. The process handled by the velocity network v_θ for a single step of the sequence S_t and coordinates X_t is:

$$S_{t+1}, X_{t+1} = v_\theta(S_t, X_t) \quad (15)$$

For convenience in representing the subsequent algorithm, let S_{t+1} and X_{t+1} be denoted as $v_\theta^s(t)$ and $v_\theta^x(t)$, respectively.

4.4 Training and Sampling

Loss. The total loss of the model, in addition to the flow loss \mathcal{L}_F defined in Equation (7), also incorporates losses measuring the differences between the generated antibody (both sequence and structure) and the ground truth. These include sequence loss \mathcal{L}_{seq} , structure loss \mathcal{L}_{struct} , and docking loss \mathcal{L}_{dock} that indicates the quality of the docking interface. More details about the loss are presented in Appendix F.

$$\mathcal{L} = \mathcal{L}_F + \mathcal{L}_{seq} + \mathcal{L}_{struct} + \mathcal{L}_{dock}. \quad (16)$$

We further note that the flow loss \mathcal{L}_F , defined in Equation 7, can also be interpreted as a constraint on the docking interface. This arises because the true velocity field in \mathcal{L}_F inherently models the temporal evolution of paratope coordinates during the flow-matching

process, while the velocity field network v_θ simultaneously predicts these coordinates updates.

Here we present the training algorithm in Algorithm 1 according to the model mentioned above. The input data includes the sequences of antibodies and specific antigenic epitope data. The objective is to learn how to generate antibody structures and sequences that meet expectations by optimizing the model parameter θ .

Algorithm 1 Training Algorithm of AbFlow

```

1: Input: antibody and specific-antigen epitope data, where the
   paratope data distribution is denoted as  $\rho_1$ .
2: Initialize: vector field network  $v_\theta$ , initial Gaussian noise  $\rho_0$ 
3: while  $\theta$  has not converged do
4:    $t \sim \mathcal{U}(0, 1)$ ,  $X_0 \sim \rho_0$ ,  $X_1 \sim \rho_1$ 
5:    $\vec{R}, \vec{t}, \vec{\pi} = \arg \min_{R, t, \pi} \|X_1 - \pi(RX_0 + t)\|^2$ 
6:    $\hat{X}_0 = \vec{\pi}(\vec{R}X_0 + \vec{t})$ 
7:    $x_t = [1 - (1 - \sigma_{\min})t]\hat{X}_0 + tX_1$ 
8:    $\mathcal{L}_F = \mathbb{E}_{t, X_0, X_1 \sim \Gamma(\rho_0, \rho_1)} \left\| v_\theta^x(t) - \left( X_1 - (1 - \sigma_{\min})\hat{X}_0 \right) \right\|^2 \triangleright \text{Eq. 7}$ 
9:    $\mathcal{L} = \mathcal{L}_F + \mathcal{L}_{\text{seq}} + \mathcal{L}_{\text{struct}} + \mathcal{L}_{\text{dock}} \triangleright \text{Eq. 16}$ 
10: end while
11: return  $v_\theta$ 

```

In the Algorithm 2, we describe the sampling process of the AbFlow model. This process is based on an ordinary differential equation (ODE) solver and obtains the target antibody structure from the noise by guiding the generation process.

Algorithm 2 Sampling Algorithm of AbFlow

```

Input: vector field model  $v_\theta$ , sampling steps  $n_s$ 
2:  $X_0 \sim \mathcal{N}(0, I)$ ,  $S_0 = [\text{MASK}]$ ,  $\Delta t = 1/n_s$ 
   for  $t = 0, \Delta t, \dots, 1 - \Delta t$  do
4:    $X_{t+\Delta t} = X_t + v_\theta^x(t) \triangleright \text{ODE solution}$ 
    $S_{t+\Delta t} = S_t + v_\theta^s(t)$ 
6:   end for
    $\hat{X}_1, \hat{S}_1 \leftarrow v_\theta(X_1, S_1)$ 
8: //Perform message passing from paratope to the entire antibody
   again after the final step.
   return  $\hat{X}_1, \hat{S}_1$ 

```

Note that during both training and sampling, the input and output of v_θ are the entire antibody's sequence and structure, and the paratope of the structure is extracted to serve as the flow for transport of probability distribution and ODE-based sampling.

5 Experiments

To validate the effectiveness of our proposed AbFlow, we conducted experiments on 4 critical tasks related to antibody generation: 1) paratope-centric antibody design (5.2), multi-CDRs and full-atom antibody design (5.3), binding affinity optimization (5.4), and complex structure prediction (5.5). We also provide details of our experimental setups (in 5.1) and ablation studies on key modules (in Section 6) to verify their contributions.

5.1 Experiment Setup

Datasets. The experiments are trained on the Structural Antibody Database (SAbDab) [10]. For the full-atom antibody design task, the RAbD benchmark [2] composed of 60 diverse complexes selected by domain experts is used for test. For the affinity optimization task, antibodies from SKEMPI V2.0 [17] are used for evaluation. We confirm that there are no duplicate samples between the training set and the test set to avoid data leakage. More details about the dataset are presented in Appendix B.

Baselines. For end-to-end full-atom antibody design methods, we use three representative baselines spanning different generative paradigms: dyMEAN [22] (GNN-based), IgGM [45] (diffusion-based), and dyAb [44] (flow-based). For other models used in CDR-H3 generation, including RosettaAb [2], MEAN [21], DiffAb [28], and HERN [18], we standardized the remaining steps of the step-by-step pipeline to ensure a fair comparison with our AbFlow. Specifically, we use IgFold [36] for antibody structure prediction, HDock [49] for antigen-antibody docking, and Rosetta [4] is used for side-chain packing. Here we use IgFold instead of AlphaFold [19] due to its specialization in antibody structure prediction.

Metrics. For the full-atom antibody design task, we employed metrics evaluating sequence recovery (AAR, CAAR [35]) and structural similarity (TM-score [48, 50], IDDT [30], RMSD [20], DockQ [6, 31]) to assess the quality of generated antibody structures in terms of both structural fidelity and antigen-antibody docking interface geometry. For the binding affinity optimization task, we utilized binding free energy change ($\Delta\Delta G$) [39] and IMP to quantify optimization efficacy and success rates. Detailed definitions of these evaluation metrics are provided in Section 5.3 and Appendix C.

5.2 Paratope-centric Antibody Design

This task is the main experiment outlined in Section 3, which involves the co-design of the 1D CDR-H3 sequence and the 3D coordinates of the full-atom antibody. We compare our AbFlow model with several baseline methods. As shown in Table 1, AbFlow achieves the best performance across most evaluation metrics. This includes both the entire antibody structure (TMscore, IDDT) and the CDR-H3 sequence along with its interface with the epitope (CAAR, DockQ). Notably, the RMSD reported here corresponds to the entire antigen-antibody complex after structural alignment of the CDR-H3 region. This alignment is performed to focus on the quality of the entire antibody structure, with particular attention to the CDR-H3 region, which plays a central role in antigen binding. Additionally, we also evaluated AbFlow on the updated DockQ v2 [31] across the entire test set, where AbFlow scored 0.339 compared to dyMEAN's 0.332, further demonstrating AbFlow's superior performance.

To assess the stability of our model, we also provide results from multiple sampling called AbFlow-G(Generator), where 30 samples were generated for each test target. The results demonstrate high consistency across repeated trials, highlighting the robustness of the model, which is enabled by the deterministic flow matching mechanism that ensures stable trajectory generation while maintaining efficient sampling.

Figure 3 presents a case study from our full-atom antibody design task. In this case, the SME module enhances the interaction between

Table 1: Comparison of Different Models on the Paratope-centric Antibody Design Task. AbFlow results include standard deviations and their corresponding 2σ confidence coverage to reflect statistical stability.

Model	Overall			Interface		
	AAR↑	TMscore↑	IDDT↑	CAAR↑	RMSD↓	DockQ↑
RosettaAb [2]	0.3231	0.9717	0.8272	0.1458	17.70	0.137
DiffAb [28]	0.3531	0.9695	0.8281	0.2217	23.24	0.158
MEAN [21]	0.3738	0.9688	0.8252	0.2411	17.30	0.162
HERN [18]	0.3265	-	-	0.1927	9.15	0.294
dyMEAN [22]	0.4365	0.9726	0.8454	0.2811	8.11	0.409
dyAb [44]	0.3789	0.9264	0.6957	0.2614	9.86	0.342
AbFlow	0.4234 ± 0.1334 (96.7%)	0.9736 ± 0.009 (93.3%)	0.8522 ± 0.0216 (95%)	0.2824 ± 0.2037 (96.7%)	8.25 ± 4.55 (98.3%)	0.423 ± 0.161 (93.3%)
AbFlow-G	0.4204	0.9736	0.8522	0.279	8.28	0.422

the epitope and the paratope. Compared to dyMEAN, AbFlow better avoids steric clashes in the generated structure, which is crucial for improving the rationality and stability of the antibody design. Reducing steric clashes—defined as the undesirable overlap between atoms—leads to more physically plausible structures and improves the quality of the antigen-antibody interface, which better reflects the true nature of their interaction.

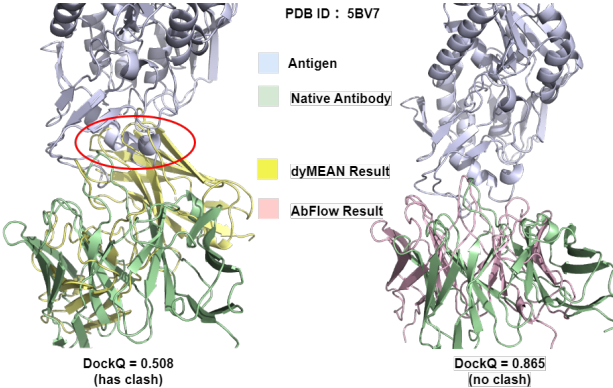


Figure 3: Case Study of the Full-atom Antibody Design Task. The structures on the left and right show antibodies generated by dyMEAN and AbFlow, respectively. The antibody designed by dyMEAN (yellow) exhibits a distinct steric clash (red circle) with the epitope, while AbFlow (pink) effectively avoids this clash, generating a structure highly similar to the true antibody (green).

5.3 Multi-CDRs and Full-atom Antibody Design

To evaluate the scalability of AbFlow beyond CDR-H3 generation, we further conduct multi-CDR design experiments on the RAbD test set, covering all six CDRs (H1–H3, L1–L3). As shown in Table 2, AbFlow consistently achieves the lowest RMSD across all CDRs, demonstrating its ability to model cross-CDR structural dependencies and maintain global structural coherence even when multiple loops are generated simultaneously. Our AbFlow outperforms DiffAb [28], dyMEAN [22], and AbX [53] by a clear margin on both

heavy-chain and light-chain loops. These results confirm that the paratope-restricted flow matching and EGNN-based refinement in AbFlow generalize effectively to multi-region antibody design.

Beyond CDR-level evaluation, we further assess AbFlow on full-atom antibody structure prediction, where only dyMEAN provides comparable baselines among existing end-to-end methods. As presented in Table 2, AbFlow achieves superior performance on all global structural metrics, including RMSD, TMscore, IDDT, and DockQ, highlighting its advantage in generating accurate and coherent full-antibody structures.

Table 2: Multi-CDRs and full-atom design results.

Multi-CDRs Results				
Method	CDR (H)	RMSD ↓	CDR (L)	RMSD ↓
DiffAb	H1	0.88	L1	0.85
dyMEAN		1.09		1.03
AbX		0.85		0.78
AbFlow	0.63	0.64		
DiffAb	H2	0.78	L2	0.55
dyMEAN		1.11		0.66
AbX		0.76		0.45
AbFlow	0.55	0.25		
DiffAb	H3	2.86	L3	1.39
dyMEAN		3.88		1.44
AbX		2.50		1.18
AbFlow	1.83	0.65		
Full-atom Results				
	RMSD ↓	TMscore ↑	IDDT ↑	DockQ ↑
dyMEAN	1.357	0.9653	0.8028	0.396
AbFlow	1.102	0.9707	0.8151	0.431

5.4 Binding Affinity Optimization

Antibody binding affinity optimization is essential for enhancing the interaction between antibodies and their target antigens, improving specificity and efficacy while minimizing off-target effects. To achieve this, it is crucial to optimize the binding affinity by altering as few residues as possible. In this task, we use $\Delta\Delta G$ as a key metric to evaluate the optimization effect, which represents the change in binding affinity, and ΔL , which tracks the number of

residues altered after optimization. These $\Delta\Delta G$ values are predicted using a GNN-based model, which is further refined by training a multi-layer perceptron (MLP) to improve accuracy. Additionally, we introduce the IMP (IMprovement Percentage), which quantifies the proportion of improvement in binding affinity achieved after optimization.

Table 3: Affinity Optimization Comparison of Different Models.

	Best $\Delta\Delta G \downarrow$	$\Delta L \downarrow$	$IMP(\%) \uparrow$
DiffAb [28]	-2.17	7.06	-
MEAN [21]	-6.48	8.96	-
dyMEAN [22]	<u>-7.7</u>	4.92	36.7%
AbFlow	-16.46	<u>6.79</u>	38.4%

Table 3 presents a comparison of our AbFlow model with other methods, including DiffAb [28], MEAN [21], and dyMEAN [22], across three key metrics: best $\Delta\Delta G$, ΔL , and IMP. The results show that AbFlow outperforms the other methods in terms of both reducing the changes in binding affinity and minimizing the number of altered residues. Furthermore, AbFlow achieves a higher IMP, indicating a greater proportion of improvement in binding affinity. These results highlight that AbFlow is not only effective in optimizing the binding affinity but also makes acceptable structural changes to the antibody.

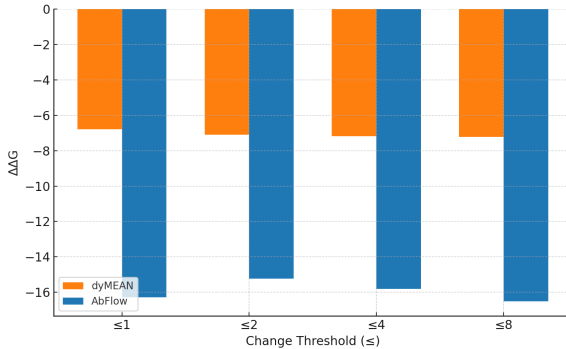


Figure 4: $\Delta\Delta G$ Comparison at Different Length of Changed Residues.

Figure 4 presents a comparison of affinity optimization results when the number of changed residues is constrained. Specifically, the optimization was performed under various thresholds, limiting the maximum number of residues that could be altered to 1, 2, 4, and 8. The figure compares the performance of AbFlow with dyMEAN across these different thresholds. It shows that AbFlow maintains stable optimization performance, consistently achieving favorable $\Delta\Delta G$ values, even when the number of residues altered is limited.

5.5 Complex Structure Prediction

We also evaluated the performance of AbFlow on the complex structure prediction task, specifically in predicting the antigen-antibody complex structure given the complete antibody sequences.

The results were compared to those of HDock [49], HERN [18], dyMEAN [22], and AlphaFold 3 [1]. Notably, both HDock and HERN are docking methods, requiring first the prediction of the antibody structure using IgFold [36], followed by docking the antigen and antibody using their respective methods, and then assembling the side-chain with Rosetta. In contrast, AlphaFold 3 directly predicts the complex structure when provided with the sequences of both the antigen and the antibody.

Table 4: Antigen-antibody Structure Prediction Comparison of Different Models.

Model	TMscore↑	IDDT↑	RMSD ↓	DockQ↑
HDock [49]	0.9701	0.8439	16.32	0.202
HERN [18]	0.9702	0.8441	9.63	0.429
dyMEAN [22]	0.9731	0.8673	<u>9.05</u>	<u>0.452</u>
AlphaFold 3 [1]	0.9799	0.921	9.47	0.475
AbFlow	<u>0.9714</u>	<u>0.8618</u>	9.01	0.455

Interestingly, our tests also revealed that AbFlow performs better when the flow model’s sampling process is omitted. By using only the velocity network as an encoder, we achieved superior results, showing that this simplified approach can enhance the overall performance of end-to-end protein structure prediction tasks.

We evaluated the methods using TM-score, IDDT, and DockQ, as shown in Table 4. Our results indicate that AbFlow outperforms all methods except AlphaFold3 in terms of docking metrics (RMSD DockQ), which reflects the quality of interaction prediction. While AlphaFold3 excels at predicting monomer structures, it leaves room for improvement in protein complex predictions. The gap between our method and AlphaFold3, in this regard, is not insurmountable, providing a clear direction for future development.

6 Ablation Study

In this section, we evaluate the effects of the proposed framework and modules in AbFlow, as well as the influence of sampling steps.

Table 5 presents the results of the ablation study for the full-atom antibody design task. The results demonstrate that both the flow matching and SME module significantly enhance the generation of full-atom antibodies. The **w/o Flow** setting refers to a scenario where the flow matching framework is not used, and the model is reduced to an end-to-end prediction model, with the velocity network serving as the encoder. This setting indicates that the velocity field network v_θ in the flow matching framework ensures the overall accuracy of sequence-structure co-design. And the **w/o SME** indicates that the SME module notably improves the interface quality.

We also show the sampling efficiency by choosing different sampling steps ($n_s = 10, 20, 50$) in Table 5. The results demonstrate that our method achieves superior performance with fewer generation steps, primarily due to the focused modeling of flow transport exclusively on the paratope region. This region typically spans 10-20 residues in length, and the average length of the test set is 13 residues. Compared to [14], which targets small-molecule 3D conformer generation. Notably, our approach attains protein-level generation efficiency comparable to small-molecule methods.

Table 5: Ablation Study Results on the Full-atom Antibody Design

	AAR↑	TMscore↑	IDDT↑	CAAR↑	RMSD↓	DockQ↑
AbFlow	0.4234	0.9736	0.8522	0.2824	8.25	0.423
w\o Flow	0.4	0.9721	0.8448	0.264	7.76	0.417
w\o SME	0.4046	0.9732	0.8506	0.2602	8.12	0.335
AbFlow-10	0.4234	0.9736	0.8522	0.2824	8.25	0.423
AbFlow-20	0.4178	0.9736	0.8522	0.277	8.26	0.424
AbFlow-50	0.4213	0.9736	0.8521	0.2812	8.29	0.42

Table 6: Ablation Study Results on the Affinity Optimization

	Best $\Delta\Delta G \downarrow$	$\Delta L \downarrow$	$IMP\% \uparrow$
AbFlow	-16.46	6.79	38.4%
w\o Flow	-5.41	2.59	40%
w\o SME	-5.71	4.41	40.8%
dyMEAN	-7.7	4.92	36.7%

Table 6 presents the ablation study results of AbFlow on the binding affinity optimization task. The results show that the complete AbFlow model significantly improves the affinity optimization performance. Even though it tends to change more residues, the resulting improvement in $\Delta\Delta G$ is substantial. We believe that the optimization gains achieved at the cost of ΔL are acceptable.

7 Computational Efficiency

To assess the computational efficiency of AbFlow, we compare both its theoretical complexity and empirical runtime against predictive end-to-end methods as well as step-by-step generative baselines.

Compared with dyMEAN, AbFlow performs flow matching-based sampling rather than single-step predictive inference. This inevitably introduces a sampling step T and a dependence on the number of sampled surface vertices M_0 —an overhead that can be further optimized in future work. Even with this acceptable increase in computational cost, as shown in Table 7, AbFlow achieves substantially stronger structural performance, representing a favorable trade-off relative to dyMEAN’s simpler predictive formulation.

When compared with step-by-step methods such as DiffAb, AbFlow demonstrates advantages in both accuracy and efficiency. DiffAb requires 13.s for CDR-H3 diffusion plus 9.89.s for template generation (22.89.s total), whereas AbFlow completes full-atom generation in comparable or less time while producing significantly better structures. These results highlight that restricting flow matching to the paratope and coupling it with EGNN refinement yields an efficient and effective framework for full-atom antibody design.

Table 7: Comparison of training and inference efficiency per sample across models.

Model	Train (s)	Infer (s)	Model	Infer (s)
AbFlow	4.56	1.4 (per step)	AbFlow	14
dyMEAN	2.21	0.47	DiffAb	22.89

8 Future Work

While our method demonstrates promising results, several limitations remain to be addressed. The surface information aggregation mechanism, though effective for capturing geometric and physico-chemical features, introduces computational overhead that prolongs inference time and may limit real-time or high-throughput applications. A promising direction for future work is to develop adaptive surface sampling strategies—dynamically selecting an appropriate number of surface vertices for each epitope based on its geometry—to further reduce computational cost while preserving the fidelity of geometric information.

On the application side, our problem setting assumes CDR-dominated binding, which limits applicability to cases where framework–epitope interactions are essential. Extending AbFlow to handle such framework-dominated regimes represents an important direction for future work. In addition, although our study focuses on antibodies, extending the framework to broader protein complexes (e.g., protein–ligand or peptide binders) remains an open challenge. Such generalization would further expand the applicability of our approach to wider protein engineering tasks.

9 Conclusion

In this study, we introduced AbFlow, an end-to-end flow-matching framework designed to optimize the full-atom antibody design process. By leveraging paratope-centric distribution transport and enhancing the velocity field network with an equivariant Surface Multi-channel Encoder (SME), AbFlow offers efficient full-atom antibody design. Our experiments demonstrate that AbFlow significantly outperforms existing generative and predictive methods in generating structurally accurate antibodies with improved binding affinity. Furthermore, AbFlow is poised to accelerate the development of therapeutic antibodies, especially in scenarios requiring rapid responses to emerging diseases or the creation of personalized immunotherapies.

Acknowledgments

This research was supported in part by National Natural Science Foundation of China (No. 92470128, No. U2241212, No.62376276), by Beijing Nova Program (No. 20230484278). We also wish to acknowledge the support provided by the fund for building world-class universities (disciplines) of Renmin University of China, by Intelligent Social Governance Interdisciplinary Platform, Major Innovation & Planning Interdisciplinary Platform for the “Double-First Class” Initiative, Public Policy and Decision-making Research Lab, and Public Computing Cloud, Renmin University of China.

References

[1] Josh Abramson, Jonas Adler, Jack Dunger, Richard Evans, Tim Green, Alexander Pritzel, Olaf Ronneberger, Lindsay Willmore, Andrew J Ballard, Joshua Bambrick, et al. 2024. Accurate structure prediction of biomolecular interactions with AlphaFold 3. *Nature* 630, 8016 (2024), 493–500.

[2] Jared Adolf-Bryfogle, Oleks Kalyuzhnii, Michael Kubitz, Brian D Weitzner, Xiaozhen Hu, Yumiko Adachi, William R Schief, and Roland L Dunbrack Jr. 2018. RosettaAntibodyDesign (RAbD): A general framework for computational antibody design. *PLoS computational biology* 14, 4 (2018), e1006112.

[3] Michael S. Albergo and Eric Vanden-Eijnden. 2023. Building Normalizing Flows with Stochastic Interpolants. arXiv:2209.15571 [cs.LG] <https://arxiv.org/abs/2209.15571>

[4] Rebecca F Alford, Andrew Leaver-Fay, Jeliazko R Jeliazkov, Matthew J O'Meara, Frank P DiMaio, Hahnbeom Park, Maxim V Shapovalov, P Douglas Renfrew, Vikram K Mulligan, Kalli Kappel, et al. 2017. The Rosetta all-atom energy function for macromolecular modeling and design. *Journal of chemical theory and computation* 13, 6 (2017), 3031–3048.

[5] Juan C Almagro, Tracy R Daniels-Wells, Sonia Mayra Perez-Tapia, and Manuel L Penichet. 2018. Progress and challenges in the design and clinical development of antibodies for cancer therapy. *Frontiers in immunology* 8 (2018), 1751.

[6] Sankar Basu and Björn Wallner. 2016. DockQ: a quality measure for protein-protein docking models. *PLoS one* 11, 8 (2016), e0161879.

[7] Igor B Buchwalow and Werner Böcker. 2009. Antibodies for immunohistochemistry. In *Immunohistochemistry: Basics and methods*. Springer, 1–8.

[8] Yoonjoo Choi, Casey Hua, Charles L Sentman, Margaret E Ackerman, and Chris Bailey-Kellogg. 2015. Antibody humanization by structure-based computational protein design. In *MAbs*, Vol. 7. Taylor & Francis, 1045–1057.

[9] Jacqueline Douglass, Emily Han-Chung Hsieh, Brian J Mog, Michael S Hwang, Sarah R DiNapoli, Alexander H Pearlman, Michelle S Miller, Katharine M Wright, P Aitana Azurmendi, Qing Wang, et al. 2021. Bispecific antibodies targeting mutant RAS neoantigens. *Science immunology* 6, 57 (2021), eabd5515.

[10] James Dunbar, Konrad Krawczyk, Jinwoo Leem, Terry Baker, Angelika Fuchs, Guy Georges, Jiye Shi, and Charlotte M Deane. 2014. SAbDab: the structural antibody database. *Nucleic acids research* 42, D1 (2014), D1140–D1146.

[11] Gero Friesecke. 2024. *Optimal Transport: A Comprehensive Introduction to Modeling, Analysis, Simulation, Applications*. Society for Industrial and Applied Mathematics, Philadelphia, PA. arXiv:<https://pubs.siam.org/doi/pdf/10.1137/1.9781611978094> doi:10.1137/1.9781611978094

[12] Tianfan Fu and Jimeng Sun. 2022. Antibody complementarity determining regions (cdrs) design using constrained energy model. In *Proceedings of the 28th ACM SIGKDD conference on knowledge discovery and data mining*, 389–399.

[13] Pablo Gainza, Freyr Sverrisson, Frederico Monti, Emanuele Rodola, Davide Boscaini, Michael M Bronstein, and Bruno E Correia. 2020. Deciphering interaction fingerprints from protein molecular surfaces using geometric deep learning. *Nature Methods* 17, 2 (2020), 184–192.

[14] Majdi Hassan, Nikhil Shenoy, Jungyoon Lee, Haines Stark, Stephan Thaler, and Dominique Beaini. 2024. ET-Flow: Equivariant Flow-Matching for Molecular Conformer Generation. arXiv:2410.22388 [q-bio.QM] <https://arxiv.org/abs/2410.22388>

[15] Jonathan Ho, Ajay Jain, and Pieter Abbeel. 2020. Denoising diffusion probabilistic models. *Advances in neural information processing systems* 33 (2020), 6840–6851.

[16] Haokai Hong, Wanyi Lin, and Kay Chen Tan. 2025. Accelerating 3D Molecule Generation via Jointly Geometric Optimal Transport. arXiv:2405.15252 [cs.LG] <https://arxiv.org/abs/2405.15252>

[17] Justina Jankauskaitė, Brian Jiménez-García, Justas Dapkūnas, Juan Fernández-Recio, and Iain H Moal. 2019. SKEMPI 2.0: an updated benchmark of changes in protein–protein binding energy, kinetics and thermodynamics upon mutation. *Bioinformatics* 35, 3 (2019), 462–469.

[18] Wengong Jin, Dr.Regina Barzilay, and Tommi Jaakkola. 2022. Antibody-Antigen Docking and Design via Hierarchical Structure Refinement. In *Proceedings of the 39th International Conference on Machine Learning*, Vol. 162. PMLR, 10217–10227.

[19] John Jumper, Richard Evans, Alexander Pritzel, Tim Green, Michael Figurnov, Olaf Ronneberger, Kathryn Tunyasuvunakool, Russ Bates, Augustin Žídek, Anna Potapenko, et al. 2021. Highly accurate protein structure prediction with AlphaFold. *nature* 596, 7873 (2021), 583–589.

[20] Wolfgang Kabsch. 1976. A solution for the best rotation to relate two sets of vectors. *Acta Crystallographica Section A: Crystal Physics, Diffraction, Theoretical and General Crystallography* 32, 5 (1976), 922–923.

[21] Xiangzhe Kong, Wenbing Huang, and Yang Liu. 2022. Conditional antibody design as 3d equivariant graph translation. arXiv preprint arXiv:2208.06073 (2022).

[22] Xiangzhe Kong, Wenbing Huang, and Yang Liu. 2023. End-to-end full-atom antibody design. arXiv preprint arXiv:2302.00203 (2023).

[23] Harold W Kuhn. 1955. The Hungarian method for the assignment problem. *Naval research logistics quarterly* 2, 1–2 (1955), 83–97.

[24] Tong Li, Robert J Pantazis, and Costas D Maranas. 2014. OptMAVEN—a new framework for the de novo design of antibody variable region models targeting specific antigen epitopes. *PLoS one* 9, 8 (2014), e105954.

[25] Yaron Lipman, Ricky TQ Chen, Heli Ben-Hamu, Maximilian Nickel, and Matt Le. 2022. Flow matching for generative modeling. *arXiv preprint arXiv:2210.02747* (2022).

[26] Ge Liu, Haoyang Zeng, Jonas Mueller, Brandon Carter, Ziheng Wang, Jonas Schilz, Geraldine Horny, Michael E Birnbaum, Stefan Ewert, and David K Gifford. 2020. Antibody complementarity determining region design using high-capacity machine learning. *Bioinformatics* 36, 7 (2020), 2126–2133.

[27] Xingchao Liu, Chengyue Gong, and Qiang Liu. 2022. Flow Straight and Fast: Learning to Generate and Transfer Data with Rectified Flow. arXiv:2209.03003 [cs.LG] <https://arxiv.org/abs/2209.03003>

[28] Shitong Luo, Yufeng Su, Xingang Peng, Sheng Wang, Jian Peng, and Jianzhu Ma. 2022. Antigen-specific antibody design and optimization with diffusion-based generative models for protein structures. *Advances in Neural Information Processing Systems* 35 (2022), 9754–9767.

[29] Robert M MacCallum, Andrew CR Martin, and Janet M Thornton. 1996. Antibody-antigen interactions: contact analysis and binding site topography. *Journal of molecular biology* 262, 5 (1996), 732–745.

[30] Valerio Mariani, Marco Biasini, Alessandro Barbato, and Torsten Schwede. 2013. IDDT: a local superposition-free score for comparing protein structures and models using distance difference tests. *Bioinformatics* 29, 21 (2013), 2722–2728.

[31] Claudio Mirabello and Björn Wallner. 2024. DockQ v2: Improved automatic quality measure for protein multimers, nucleic acids, and small molecules. *Bioinformatics* 40, 10 (2024), btae586.

[32] Sanjay Nagaraj, Amir Shafehazzadeh, Hyun Park, Jonathan King, and Simon Levine. 2024. Igflow: Flow matching for de novo antibody design. *Advances in Neural Information Processing Systems* (2024).

[33] Kirill Neklyudov, Rob Brekelmans, Alexander Tong, Lazar Atanackovic, Qiang Liu, and Alireza Makhzani. 2023. A computational framework for solving wasserstein lagrangian flows. *arXiv preprint arXiv:2310.10649* (2023).

[34] Brian G Pierce, Yuichiro Hourai, and Zhiping Weng. 2011. Accelerating protein docking in ZDOCK using an advanced 3D convolution library. *PLoS one* 6, 9 (2011), e24657.

[35] Thiruvarangan Ramaraj, Thomas Angel, Edward A Dratz, Algirdas J Jesaitis, and Brendan Mumey. 2012. Antigen–antibody interface properties: Composition, residue interactions, and features of 53 non-redundant structures. *Biochimica et Biophysica Acta (BBA)-Proteins and Proteomics* 1824, 3 (2012), 520–532.

[36] Jeffrey A Ruffolo, Lee-Shin Chu, Sai Pooja Mahajan, and Jeffrey J Gray. 2023. Fast, accurate antibody structure prediction from deep learning on massive set of natural antibodies. *Nature communications* 14, 1 (2023), 2389.

[37] Koichiro Saka, Taro Kakuzaki, Shoichi Metsugi, Daiki Kashiwagi, Kenji Yoshida, Manabu Wada, Hiroyuki Tsunoda, and Reiji Teramoto. 2021. Antibody design using LSTM based deep generative model from phage display library for affinity maturation. *Scientific reports* 11, 1 (2021), 5852.

[38] Michel F Sanner, Arthur J Olson, and Jean-Claude Spehner. 1996. Reduced surface: an efficient way to compute molecular surfaces. *Biopolymers* 38, 3 (1996), 305–320.

[39] Sisi Shan, Shitong Luo, Ziqing Yang, Junxian Hong, Yufeng Su, Fan Ding, Lili Fu, Chenyu Li, Peng Chen, Jianzhu Ma, et al. 2022. Deep learning guided optimization of human antibody against SARS-CoV-2 variants with broad neutralization. *Proceedings of the National Academy of Sciences* 119, 11 (2022), e2122954119.

[40] Yang Song, Conor Durkan, Iain Murray, and Stefano Ermon. 2021. Maximum likelihood training of score-based diffusion models. *Advances in neural information processing systems* 34 (2021), 14115–14228.

[41] Zhenqiao Song, Tinglin Huang, Lei Li, and Wengong Jin. 2024. SurfPro: Functional Protein Design Based on Continuous Surface. arXiv preprint arXiv:2405.06693 (2024).

[42] Freyr Sverrisson, Jean Feydy, Bruno E Correia, and Michael M Bronstein. 2021. Fast end-to-end learning on protein surfaces. In *Proceedings of the IEEE/CVF Conference on Computer Vision and Pattern Recognition*, 15272–15281.

[43] Melody A Swartz, Sachiko Hirose, and Jeffrey A Hubbell. 2012. Engineering approaches to immunotherapy. *Science translational medicine* 4, 148 (2012), 148rv9–148rv9.

[44] Cheng Tan, Yijie Zhang, Zhangyang Gao, Yufei Huang, Haitao Lin, Lirong Wu, Fandi Wu, Mathieu Blanchette, and Stan Z Li. 2025. dyAb: Flow Matching for Flexible Antibody Design with AlphaFold-driven Pre-binding Antigen. In *Proceedings of the AAAI Conference on Artificial Intelligence*, Vol. 39. 782–790.

[45] Rubo Wang, Fandi Wu, Xingyu Gao, Jiaxiang Wu, Peilin Zhao, and Jianhua Yao. 2025. IgGM: A Generative Model for Functional Antibody and Nanobody Design. In *The Thirteenth International Conference on Learning Representations*. <https://openreview.net/forum?id=zmmfsJpYeq>

[46] Yanyan Wang, Fei-Long Meng, and Leng-Siew Yeap. 2024. DNA flexibility can shape the preferential hypermutation of antibody genes. *Trends in Immunology* (2024).

[47] Yanyan Wang, Senxin Zhang, Xinrui Yang, Joyce K Hwang, Chuanzong Zhan, Chaoyang Lian, Chong Wang, Tuantuan Gui, Binbin Wang, Xia Xie, et al. 2023. Mesoscale DNA feature in antibody-coding sequence facilitates somatic hypermutation. *Cell* 186, 10 (2023), 2193–2207.

- [48] Jinrui Xu and Yang Zhang. 2010. How significant is a protein structure similarity with TM-score= 0.5? *Bioinformatics* 26, 7 (2010), 889–895.
- [49] Yumeng Yan, Huanyu Tao, Jiahua He, and Sheng-You Huang. 2020. The HDOCK server for integrated protein–protein docking. *Nature protocols* 15, 5 (2020), 1829–1852.
- [50] Yang Zhang and Jeffrey Skolnick. 2007. Scoring function for automated assessment of protein structure template quality. *PROTEINS-NEW YORK* 68, 4 (2007), 1020.
- [51] Yang Zhang, Zhewei Wei, Ye Yuan, Chongxuan Li, and Wenbing Huang. 2024. EquiPocket: an E(3)-equivariant geometric graph neural network for ligand binding site prediction. In *Proceedings of the 41st International Conference on Machine Learning* (Vienna, Austria) (ICML '24). JMLR.org, Article 2482, 19 pages.
- [52] Nan Zhao, Binging Han, Cuicui Zhao, Jinbo Xu, and Xinqi Gong. 2024. ABAG-docking benchmark: a non-redundant structure benchmark dataset for antibody–antigen computational docking. *Briefings in Bioinformatics* 25, 2 (2024), bbae048.
- [53] Tian Zhu, Milong Ren, and Haicang Zhang. 2024. Antibody Design Using a Score-based Diffusion Model Guided by Evolutionary, Physical and Geometric Constraints. In *Proceedings of the 41st International Conference on Machine Learning*, Vol. 235. PMLR, 62531–62548.

Appendix

A E(3)-Equivariance of the velocity field network

In this section, we prove the E(3)-equivariance of our proposed velocity field network. Note that [22] has already demonstrated the E(3)-equivariance of the AME module; thus, it suffices to prove the equivariance of the SME module through the following theorem.

THEOREM A.1. *Let $\{X_i^{(l)}\}_{i \in \mathcal{V}_A \cup \mathcal{V}_E}$ denote the coordinates of residue nodes and $\{X_{s_j}^{(l)}\}_{j \in \mathcal{N}_i}$ the coordinates of interacting surface points. Let $\{S_i^{(l)}\}_{i \in \mathcal{V}_A \cup \mathcal{V}_E}$ denote the hidden states of residue sequence, respectively. Then, under any Euclidean transformation $g = (Q, t) \in E(3)$, the Surface Multi-channel Encoder is E(3)-invariant with respect to sequence inputs and E(3)-equivariant with respect to coordinate inputs. Express this in formulation:*

$$S_i^{(l)} \mapsto Q S_i^{(l)} + t \Rightarrow S_i^{(l+1)} \mapsto Q S_i^{(l+1)}. \quad (17)$$

$$X_i^{(l)} \mapsto Q X_i^{(l)} + t \Rightarrow X_i^{(l+1)} \mapsto Q X_i^{(l+1)} + t. \quad (18)$$

Proof. First, it is evident that the surface vertices corresponding to a residue are determined by their relative positional relationships, and thus remain invariant under the transformation $g \in E(3)$. Meanwhile, the coordinates of surface vertices $\{X_{s_j}^{(l)}\}_{j \in \mathcal{N}_i}$ vary synchronously with the residues coordinates X_i . This implies:

$$X_i \mapsto Q X_i + t \Rightarrow X_{s_j} \mapsto Q X_{s_j} + t, \forall j \in \mathcal{N}_i. \quad (19)$$

For a residue node i and a neighboring surface node s_j , the m_{ij} is computed via

$$m_{ij} = \phi_m(S_i^{(l)}, S_{s_j}^{(l)}, \text{msg}(X_i^{(l)}, X_{s_j}^{(l)})). \quad (20)$$

Here, the message is constructed as:

$$\begin{aligned} \text{msg}(X_i^{(l)}, X_{s_j}^{(l)}) &= \phi_v \left(\frac{A_i^\top D(X_i^{(l)}, X_{s_j}^{(l)})}{D(X_i^{(l)}, X_{s_j}^{(l)}) + \epsilon} \right), \\ D[p, q] &= \|X_i^{(l)}[p, :] - X_{s_j}^{(l)}[q, :] \|_2. \end{aligned} \quad (21)$$

for each element in matrix D that indicates Euclidean distance between a residue and a surface vert, satisfies:

$$\begin{aligned} \| (Q X_i[p, :] + t) - (Q X_{s_j}[q, :] + t) \|_2 &= \| Q(X_i[p, :] - X_{s_j}[q, :]) \|_2 \\ &= \sqrt{[Q(X_i[p, :] - X_{s_j}[q, :])]^\top [Q(X_i[p, :] - X_{s_j}[q, :])] } \\ &= \sqrt{(X_i[p, :] - X_{s_j}[q, :])^\top Q^\top Q (X_i[p, :] - X_{s_j}[q, :])} \\ &= \sqrt{(X_i[p, :] - X_{s_j}[q, :])^\top (X_i[p, :] - X_{s_j}[q, :])} \\ &= \| X_i[p, :] - X_{s_j}[q, :] \|_2. \end{aligned}$$

So we have $\text{msg}(Q X_i^{(l)} + t, Q X_{s_j}^{(l)} + t) = \text{msg}(X_i^{(l)}, X_{s_j}^{(l)})$, thus m_{ij} is invariant under $g = (Q, t)$. According to the update process of S_i :

$$S_i^{(l+1)} = \phi_s(S_i^{(l)}, \sum_{j \in \mathcal{N}_i} m_{ij}). \quad (22)$$

we can prove that our SME module remains invariant with respect to the sequence hidden states S_i .

Next, applying transformation g to the geometric messages X_{ij} involved in the aggregation process, we have:

$$\begin{aligned} X_i^{(l)} - 1X_{s_j}^{(l)}[k, :] &\mapsto Q X_i^{(l)} + t - (Q 1X_{s_j}^{(l)}[k, :] + t) \\ &= Q(X_i^{(l)} - 1X_{s_j}^{(l)}[k, :]), \quad k = 1, \dots, M. \end{aligned} \quad (23)$$

thus $X_{ij} \mapsto Q X_{ij}$.

SME updates the residues coordinates by:

$$X_i^{(l+1)} = X_i^{(l)} + \frac{1}{|\mathcal{N}_i|} \sum_{j \in \mathcal{N}_i} X_{ij} \cdot \phi_e(m_{ij}). \quad (24)$$

As $X_i^{(l)} \mapsto Q X_i^{(l)} + t$, $X_{ij} \mapsto Q X_{ij}$, and $\phi_e(m_{ij})$ is invariant, we obtain:

$$X_i^{(l+1)} \mapsto Q X_i^{(l)} + t + \frac{1}{|\mathcal{N}_i|} \sum_j Q X_{ij} \cdot \phi_e(m_{ij}) = Q X_i^{(l+1)} + t. \quad (25)$$

Thus far, we have rigorously proven that the Surface Multi-channel Encoder (SME) module exhibits E(3)-equivariance with respect to the input residue coordinates.

B Data and Model Availability

All datasets and model weights are publicly available at <https://huggingface.co/wenda8759/AbFlow>, including PDB files with train-/validation/test splits and trained model weights for all experiments.

C Evaluation Metrics

We use the following several metrics to compare the performance of our AbFlow with other models on full-atom antibody design task:

Amino Acid Recovery (AAR): The overlapping ratio of the generated sequence and the ground truth.

CAAR [35]: Computes AAR restricted to binding residues whose minimum distance from epitope residues is below 6.6Å.

TMscore [48, 50]: Measures the global similarity between the generated structure and the ground truth in terms of C_α coordinates.

Local Distance Difference Test (LDDT) [30]: Contrasts the difference of the atom-wise distance between the generated structure and the ground truth to evaluate local similarity.

RMSD: Calculates the Root Mean Square Deviation regarding the absolute coordinates of CDR-H3 without Kabsch [20, 31] alignment.

DockQ: [6]: A comprehensive score for the docking quality of a complex structure.

$\Delta\Delta G$: Represents the change in Gibbs free energy of the protein complex upon mutation, reflecting the effect of the mutation on protein stability or binding affinity.

For the metrics used to evaluate binding affinity optimization in Section 5.3:

$$best\Delta\Delta G = \frac{1}{D} \sum_{d=1}^D \min_p \Delta\Delta G_{dp}, \quad (26)$$

$$mean\Delta\Delta G = \frac{1}{DP} \sum_{d=1}^D \sum_{p=1}^P \Delta\Delta G_{dp}. \quad (27)$$

D Settings of Surface Sampling

Here, we describe how the number of surface vertices on the epitope was determined. Based on the surface cutoff of 1.5 Å introduced in Section 4.2, we computed the number of surface vertices per residue across the training set and obtained an average of approximately $\overline{|\mathbb{S}|} \approx 75$. Since each residue is assigned a fixed-size surface vertex set M_0 , residues with fewer than M_0 vertices are padded with zero vectors. To ensure that most residues provide sufficient geometric information without excessive padding, we set $M_0 = \frac{2}{3} \overline{|\mathbb{S}|} \approx 50$.

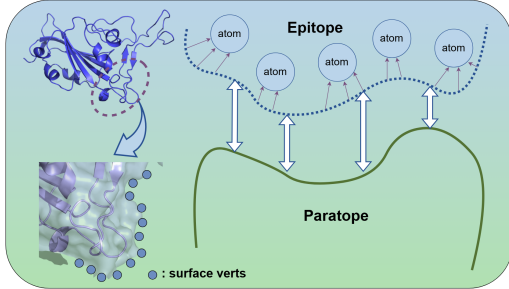


Figure 5: Schematic diagram of surface definition and message passing. We generate surface vertices within a cutoff of 1.5 Å around the epitope. For each vertex, we assign the nearest residue. Then, we perform message passing between the surface vertices and the antibody paratope using SME to enhance the learning ability of the interaction.

E Generation

After the modules described above, AbFlow performs a final decoding step to produce both sequence and structure outputs. For sequence generation, the hidden states are transformed into amino acid probabilities using a softmax over the 20 residue types. For structure generation, after all n_{layers} iterations of the velocity-field network, the predicted coordinates are aligned to the native paratope using the method of [20]. Since the full antibody structure is generated from the paratope outward, only minimal refinement is required during alignment to dock the antibody to the antigen.

F Losses

Losses. In this part, we specifically introduce the various losses that make up the Equation 16 in Section 4.4, including the three parts except for the flow matching loss \mathcal{L}_F : sequence loss \mathcal{L}_{seq} , structure loss \mathcal{L}_{struct} , and docking loss \mathcal{L}_{dock} .

The sequence loss calculates the cross-entropy loss between the predicted amino acid type $p_i^{(t)}$ in each iteration and the one-hot vector p_i^{true} of the actual type:

$$\mathcal{L}_{seq} = \frac{1}{T |\mathcal{V}_P|} \sum_{t=1}^T \sum_{i \in \mathcal{V}_P} \ell_{ce} \left(p_i^{(t)}, p_i^{true} \right). \quad (28)$$

The structure loss consists of two parts: the coordinate loss and the chemical bond loss, which measure the global and local deviations respectively. The coordinate loss calculates the huber loss between the final iteration $X_i^{(T)}$ and the ground truth X_i^{true} after alignment. The chemical bond loss calculates the huber loss between the lengths of the chemical bonds used in the structure of $X_i^{(T)}$ and the lengths of the ground truth bonds. $\mathcal{L}_{struct} = \mathcal{L}_{coord} + \mathcal{L}_{bond}$.

$$\mathcal{L}_{coord} = \frac{1}{|\mathcal{V}_A|} \sum_{v_i \in \mathcal{V}_A} \ell_{huber} \left(X_i^{(T)}, X_i^{true} \right), \quad (29)$$

$$\mathcal{L}_{bond} = \frac{1}{|\mathcal{B}|} \sum_{b \in \mathcal{B}} \ell_{huber} \left(b^{(T)}, b^{true} \right). \quad (30)$$

The docking loss focuses on the connected-paratope and calculates the coordinate loss between the connected-paratope and the native paratope as well as the distances loss of the external edges in \mathcal{E}_{EUC} .

$$\mathcal{L}_{cp} = \frac{1}{|\mathcal{V}_C|} \sum_{i \in \mathcal{V}_C} \ell_{huber} \left(X_i^{(T)}, X_i^{true} \right). \quad (31)$$

$$\mathcal{L}_{dist} = \frac{1}{T |\mathcal{V}_E| |\mathcal{V}_C|} \sum_{t=1}^T \sum_{u \in \mathcal{V}_E, v \in \mathcal{V}_C} \ell_{huber} \left(d^{(t)}(u, v), d^{true}(u, v) \right). \quad (32)$$

Where $d(u, v), d^{true}(u, v)$ respectively represent the predicted and true residues distance between $u \in \mathcal{V}_E, v \in \mathcal{V}_C$. $\mathcal{L}_{dock} = \mathcal{L}_{cp} + \mathcal{L}_{dist}$.

G Hyperparameter and Hardware Requirements

Our AbFlow is trained using the Adam optimizer within the PyTorch data-parallel framework, implemented on 2 NVIDIA A100 GPUs, each with 80GB of VRAM. The hyperparameters of the model are detailed in Table 8.

Table 8: Model hyperparameters and training configurations

Hyperparameter	Value	Description
embed_size	64	Sequence embedding size.
hidden_size	128	Hidden state dimension.
n_layers	3	Velocity field network layers.
k_neighbors	9	KNN neighbors per node.
batch_size	16	Training batch size.
M_0	50	Surface vertices per residue.
n_steps	10	ODE sampling steps.